Electronic and optical properties of anatase TiO_2

R. Asahi and Y. Taga
Toyota Central R&D Laboratories, Inc., Nagakute, Aichi 480-1192, Japan

W. Mannstadt
Fachbereich Physik, Philipps-Universitat Marburg, 35032 Marburg, Germany

A. J. Freeman
Department of Physics and Astronomy, Northwestern University, Evanston, Illinois 60208
(Received 17 August 1999; revised manuscript received 29 October 1999)

First-principles calculations using the full-potential linearized augmented plane-wave method have been performed to investigate detailed electronic and optical properties of TiO_2 in the anatase structure. The fully optimized structure, obtained by minimizing the total energy and atomic forces, are in good agreement with experiment. Stabilization of the structure by the trade off between a favorable coordination in the sp^2 hybridization and the Coulomb repulsion among oxygen atoms is also demonstrated. We calculate band structure, densities of states and charge densities, and interpret their features in terms of the bonding structure in the molecular orbital picture. The optical properties, calculated within the dipole approximation, are found to agree with recent experiments on single crystals of anatase TiO_2. Near the absorption edge, the results show a significant optical anisotropy in the components parallel and perpendicular to the c axis. We demonstrate that this large dichroism results from the existence of nonbonding d_{xy} orbitals located at the bottom of the conduction bands, which allows direct dipole transitions dominantly for the perpendicular component.

I. INTRODUCTION

Among three different crystal structures of TiO_2, rutile, anatase, and brookite, the anatase structure has attracted much attention over the last decades for its technological applications such as photovoltic solar cells and photocatalysis with promising efficiency.[1–3] In contrast to extensive studies on the rutile structure,[4–9] however, fundamental properties of the anatase structure have not been well understood. One reason may be found in the difficulty to synthesize good-quality single crystals; so far only a few groups have reported experimental results for the bulk properties of the single crystals.[10,11] Contrary to a commonly used assumption of the similarity of their electronic structures, significant differences between anatase and rutile were found in electrical, magnetic, and optical properties.[12–16] Forro *et al.* found a very shallow donor level and a high-electron mobility in anatase.[15] Tang *et al.* investigated detailed absorption edges of anatase and rutile, and confirmed that the nature of the exciton states of anatase is self trapped while that of rutile is free.[16] Recently polarized reflection spectra of single crystals of anatase were measured using synchrotron radiation.[11] The results show a substantial dielectric anisotropy between two polarizations, $\mathbf{E}\perp c$ and $\mathbf{E}\parallel c$.

Theoretical works for anatase TiO_2 have also been few.[17–19] Pseudopotential Hartree-Fock (PHF) calculations[17] provided a band structure and structural constants. The orthogonalized linear-combination-of atomic-orbitals (OLCAO) method was also employed[19] to calculate band structures and optical properties. With those results, however, there exist several points which should be clarified: (i) detailed charge densities were not presented, and the bonding structure of anatase is not clearly understood; (ii) there is significant disagreement in the band structures given by these two methods; (iii) the dielectric functions calculated by the OLCAO method do not agree with recent experiments,[11] particularly in their anisotropic behavior; (iv) the physical origins of the optical properties were not presented. Thus, it is necessary to investigate the detailed properties of anatase in relation to the above problems using a more reliable method.

This paper presents first-principles calculations of TiO_2 in the anatase structure using the full-potential linearized augmented plane-wave (FLAPW) method.[20] The results include a fully-optimized ground-state structure obtained with total energy and atomic forces, band structure, charge densities, densities of states, and optical properties within the dipole approximation. Detailed bonding structure and optical properties are then discussed in terms of the character of the states and the dipole selection rules.

II. METHODOLOGY

We employed the FLAPW method,[20] which treats all electrons and has no shape approximations for the potential and charge density. The exchange-correlation energies are treated within the local density approximation using the Hedin-Lundqvist[21] parameterization of the exchange-correlation potential. The implementation of the FLAPW method includes total energy and atomic-force[22] calculations, which allow structure optimization.[23]

The primitive unit cell of TiO_2 in the anatase structure is shown in Fig. 1. The space group of anatase is $I4_1/amd$, and the local symmetry is D_{2d}. The structure is defined by three crystallographic parameters: two lattice parameters, a, c, and the internal parameter, $u=d_{\mathrm{ap}}/c$, where d_{ap} is the apical Ti-O bond length. We obtained the ground-state structure of

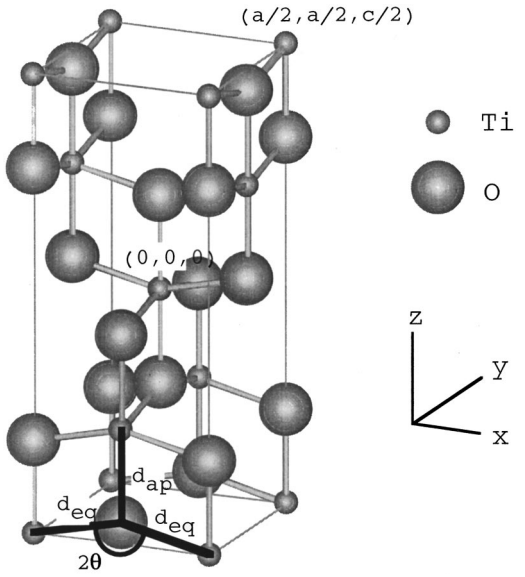

FIG. 1. Primitive unit cell and definitions of the coordinates for TiO_2 in the anatase structure. The definition of the apical (d_{ap}) and equatorial (d_{eq}) bond lengths is indicated.

anatase by minimizing the total energy with respect to the unit-cell volume, $V=ca^2$, and c/a. Each u for a set of V and c/a was decided when the force on each atom was smaller than 1 mRy/a.u.

Two energy windows were used to treat extended core states; the Ti $3s$ and $3p$ states were put in the lower semicore window, and the others were treated in the higher valence window. The valence and semicore states are solved independently by ignoring their interactions. The core states are calculated fully relativistically and updated at each iteration, whereas the valence and semicore states are treated semirelativistically, i.e., spin-orbit coupling is neglected.

Cutoffs of the plane-wave basis, 13.0 Ry, and of the potential representation, 100 Ry, and an expansion in terms of spherical harmonics with $l \leqslant 8$ inside the muffin-tin spheres, were used for the FLAPW calculations. The resulting number of plane waves was about 750. Summations over the Brillouin zone (BZ) were performed using 12 special k points[24] in the irreducible wedge for the structure optimization. Convergence was assumed when the average root-mean-square difference between the input and output charge densities was less than $1\times10^{-4}\, e/(\text{a.u.})^3$.

Optical properties were calculated within the electric-dipole approximation.[25] The imaginary parts of the dielectric functions are thus expressed by

$$\epsilon_2(\omega)=\frac{8\pi^2e^2}{\omega^2m^2V}\sum_{c,v}\sum_{\mathbf{k}}|\langle c,\mathbf{k}|\hat{\mathbf{e}}\cdot\mathbf{p}|v,\mathbf{k}\rangle|^2 \times\delta[E_c(\mathbf{k})-E_v(\mathbf{k})-\hbar\omega], \tag{1}$$

where c and v represent the conduction and valence states, $|n,\mathbf{k}\rangle$ are the eigenkets of FLAPW, $\mathbf{p}$ is the momentum operator, $\hat{\mathbf{e}}$ is the external field vector. We used 100 sampling k points in the irreducible wedge and the linear tetrahedron scheme[26] for the BZ integrations. The real parts of the dielectric functions were obtained by using the Kramers-Krönig (K-K) transformation of ϵ_2 in which a tail of the form,[27]

$$\frac{\beta\omega}{[(\hbar\omega)^2+\gamma^2]^2}, \tag{2}$$

was attached for energies greater than ω_0. In the calculations, we fixed $\gamma=4.5$ eV and $\omega_0=18$ eV, and β was determined by the continuity of ϵ_2 at ω_0.

TABLE I. Optimized structural parameters for anatase TiO_2 compared to experiment (Ref. 28) and the results of pseudopotential Hartree-Fock (PHF) calculations (Ref. 17).

	Exp.	This work	PHF
a (Å)	3.782	3.692	3.763
c (Å)	9.502	9.471	9.851
d_{eq} (Å)	1.932	1.893	1.939
d_{ap} (Å)	1.979	1.948	1.995
c/a	2.512	2.566	2.618
u	0.208	0.206	0.202
2θ	156.3°	154.4°	152.1°
V_0 (Å^3/TiO_2)	33.98	32.27	34.87

III. RESULTS AND DISCUSSION

A. Structure optimization and electronic structures

In Table I, we present our calculated optimized structure compared with experiment[28] and with the theoretical results[17] using the PHF method. In general, the agreement of the calculated structures with experiment is good. In particular, our results are in better agreement with experiment for c/a, u, and the Ti-O-Ti angle, 2θ, than PHF's, demonstrating the high accuracy of our approach. The calculated Ti-O bond lengths, d_{ap} and d_{eq}, underestimate experiment by about 2%, which is as large as the usual LDA accuracy as found in the previous results for rutile TiO_2 obtained by the pseudopotential (PP) calculations[4,6–9]— typically within 1–2 % of experiment. A method that goes beyond the local density approximation, such as the generalized gradient approximation (GGA),[29] could improve the bond lengths. In fact, the GGA correction to LDA in the PP method for rutile TiO_2 yielded an increase of the lattice parameters by 2–4 %.[9] Changes in the total energy and structural parameters as a function of c/a with a fixed volume at equilibrium, i.e., $V=V_0$, are shown in Fig. 2. Each point in the plots was obtained by minimizing the atomic forces on the atoms. We see the linear dependencies of 2θ and the O-O distance on c/a around its equilibrium value. These results serve to legitimatize a qualitative trend for distortions:[17] a preferable coordination in the planar Ti_3O units would lead to $2\theta=120°$ due to the ideal sp^2 symmetry, while a decrease in the O-O distance increases the Coulomb repulsion. It is the trade-off of these effects that yields the optimum structure.

The self-consistent band structure along the high-symmetry directions of the BZ is shown in Fig. 3. The top of the valence band is taken as the energy zero. The band structure of the present calculations is found to be quite similar to

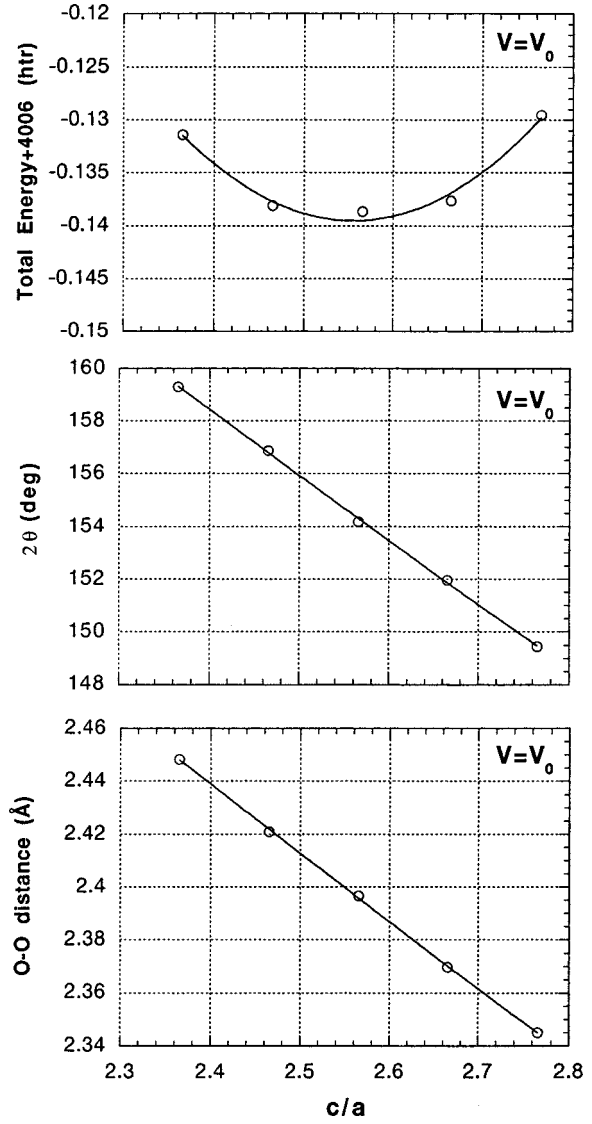

FIG. 2. Calculated total energy, 2θ, and the O-O distance as a function of c/a with the volume fixed at its equilibrium value.

that of the OLCAO calculations,[19] while that of the PHF calculations[17] is not consistent with ours even in the valence bands. We present the corresponding density of states (DOS) in Fig. 4: The lower valence bands located about -17 eV are composed predominantly of O $2s$ character. The upper valence bands show a strong hybridization between O $2p$ and Ti $3d$ electrons, and yield a band width of 5.05 eV—compared with the XPS result[12] of 4.75 eV and the OLCAO result of 5.17 eV. The conduction bands below 8 eV consist mainly of Ti $3d$ states, which show two distinct structures, below and above 5 eV. The conduction bands above 8 eV have mainly s and p character.

A minimum direct band gap was found at Γ. The energy difference in the valence-band maxima at Γ and Z was, however, only 2 meV. On the other hand, the OLCAO calculations yield an indirect transition from the valence band at M to the conduction band at Γ as the minimum band gap. Note that only the unit-cell volume of the structural parameters was optimized in the OLCAO calculations, and that we obtained the same indirect transition, $M \rightarrow \Gamma$, for the system when we used the experimental lattice parameters. Whether

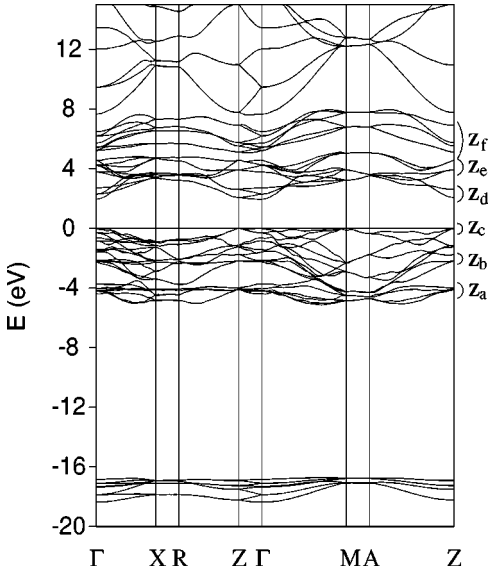

FIG. 3. Calculated band structure of the anatase TiO_2 structure. The top of the valence band is taken as the zero of energy. The labeling of states at the Z point is given for later reference.

the band gap is direct or indirect is, therefore, quite sensitive to the crystal configuration. The band gap obtained, 2.0 eV, is much smaller than experiment, 3.2 eV,[14] due to the well-known shortcoming of LDA.[30]

To examine the chemical bonding of anatase, we decomposed the DOS into Ti e_g, Ti t_{2g} (d_{yz}, d_{zx}, and d_{xy}), O p_σ (in the Ti_3O cluster plane), and O p_π (out of the Ti_3O cluster plane) contributions as shown in Fig. 4. The upper valence

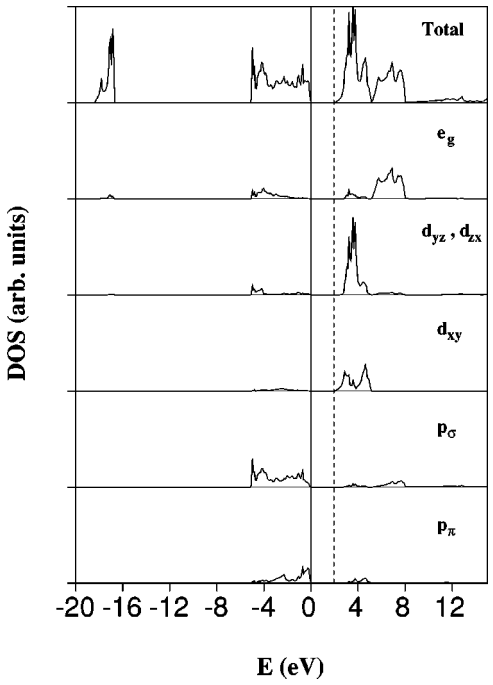

FIG. 4. Total and projected densities of states (DOS) of the anatase TiO_2 structure. The DOS is decomposed into Ti e_g, Ti t_{2g} (d_{yz}, d_{zx}, and d_{xy}), O p_σ (in the Ti_3O cluster plane), and O p_π (out of the Ti_3O cluster plane) components. The top of the valence band (the vertical solid line) is taken as the zero of energy. The vertical dashed line indicates the conduction-band minimum as a guide to the eye.

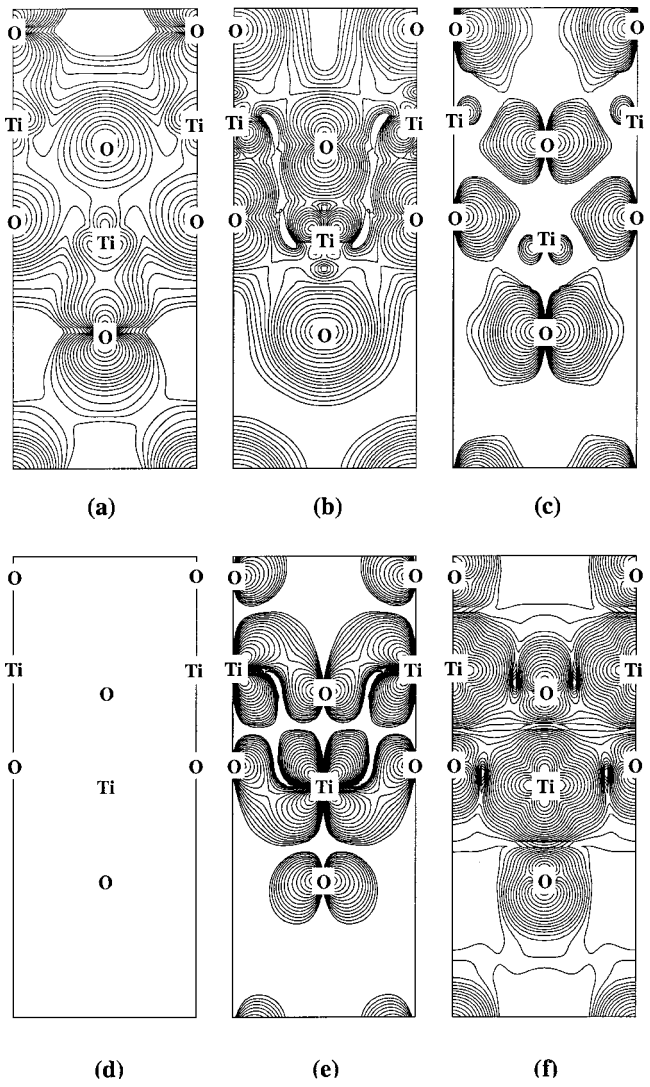

FIG. 5. Electron densities at the Z point (defined in Fig. 3) of anatase TiO_2 in the (010) plane passing through the origin: (a) valence-band states, Z_a; (b) valence-band states, Z_b; (c) valence-band states, Z_c; (d) conduction-band states, Z_d; (e) conduction-band states, Z_e; (f) conduction-band states, Z_f. The contours start from 1×10^{-3} electrons/a.u.^{3} and change successively by a factor of $\sqrt{2}$.

bands can be decomposed into three main regions: the σ bonding in the lower energy region where O p_σ mainly contributes to the bonding; the π bonding in the middle energy region; and O p_π states in the higher energy region where the hybridization with d states is almost negligible, leaving O p_π states non-bonding at the top of the valence bands. The contribution of the π bonding is much weaker than that of the σ bonding. The conduction bands are decomposed into Ti e_g (>5 eV) and t_{2g} bands (<5 eV). A significant feature of anatase can be seen at the bottom of the conduction bands (the vertical dashed line in Fig. 4) where the d_{xy} states are dominantly located. The rest of the t_{2g} bands are antibonding with p states. The main peak of the t_{2g} bands is identified to be mostly d_{yz} and d_{zx} states.

We present the charge densities of the band states at Z in Figs. 5 (in the (010) plane passing through the origin) and 6 (in the (001) plane passing through the origin) to illustrate

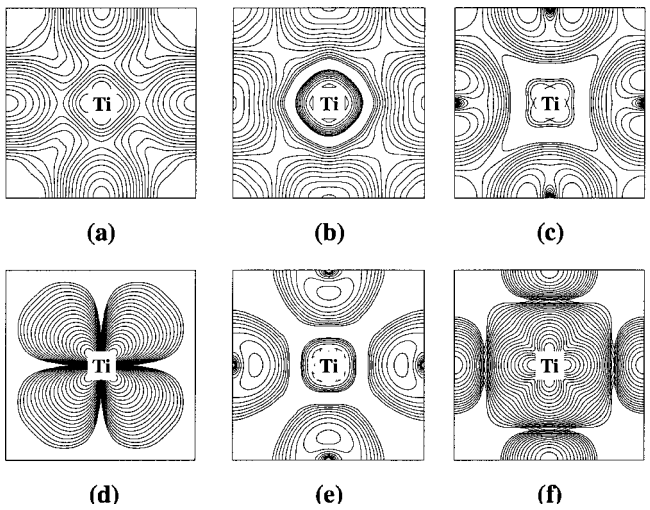

FIG. 6. The same quantities as in Fig. 5, but in the (001) plane.

the detailed bonding structure, where the states, Z_a to Z_f, are defined in Fig. 3. The features of the partial DOS described above are clearly seen in the charge densities. The most stable bonding located at the bottom of the upper valence bands, (a), is the σ bonding in the plane of the Ti_3O cluster arising from hybridization of the O p_σ and Ti e_g orbitals. The next higher valence states, (b), indicate π bonding in the apical direction from the hybridization of the O p_π and Ti d_{zx} (or d_{yz}) orbitals. The top of the valence bands, (c), is dominantly from the O p_π orbitals. The bottom of the conduction bands consists significantly of the isolated Ti d_{xy} orbitals as shown in (d). In (e), we observe the Ti d_{zx} (or d_{yz}) orbitals which are antibonding with the p_π orbitals in the apical direction, and also weakly bonding with the p_σ orbitals in the equatorial direction. This weak bonding results in slightly induced p_σ character in the t_{2g} bands, as seen in Fig. 4. The Ti e_g orbitals antibonding with the O p_σ orbitals are clearly shown in (f).

A molecular-orbital bonding diagram, derived from the character of the states as discussed above, is presented in Fig. 7. A noticeable feature can be found in the nonbonding states near the band gap: the nonbonding O p_π orbital at the top of the valence bands and the nonbonding d_{xy} states at the bottom of the conduction bands. A similar feature can be seen in rutile where, however, it is less significant than in anatase.[5] In rutile, each octahedron shares corners with eight neighbors, and shares edges with two other neighbors, forming a linear chan. On the other hand, in anatase, each octahedron shares corners with four neighbors, and shares edges with four other neighbors, forming a zigzag chain with a screw axis. Thus, anatase is less dense than rutile. Also anatase has a large metal-metal distance of 5.35 Å. As a consequence, the Ti d_{xy} orbitals at the bottom of the conduction band are quite isolated, while the t_{2g} orbitals at the bottom of the conduction band in rutile provide the metal-metal interaction with a smaller distance of 2.96 Å.

B. Optical properties

We present the imaginary part, ϵ_2, and the real part, ϵ_1, of the calculated dielectric function in Figs. 8 and 9, respectively. The tetragonal space group allows one to evaluate two

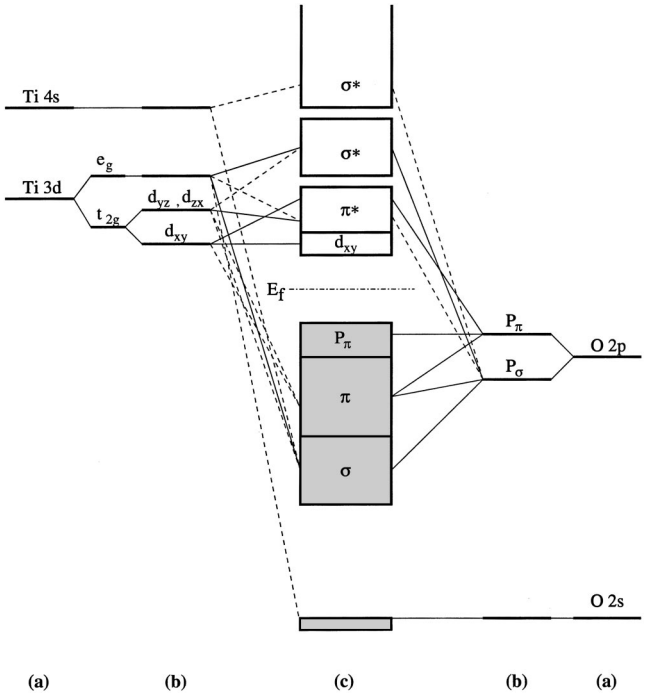

FIG. 7. Molecular-orbital bonding structure for anatase TiO_2: (a) atomic levels, (b) crystal-field split levels, and (c) final interaction states. The thin-solid and dashed lines represent large and small contributions, respectively.

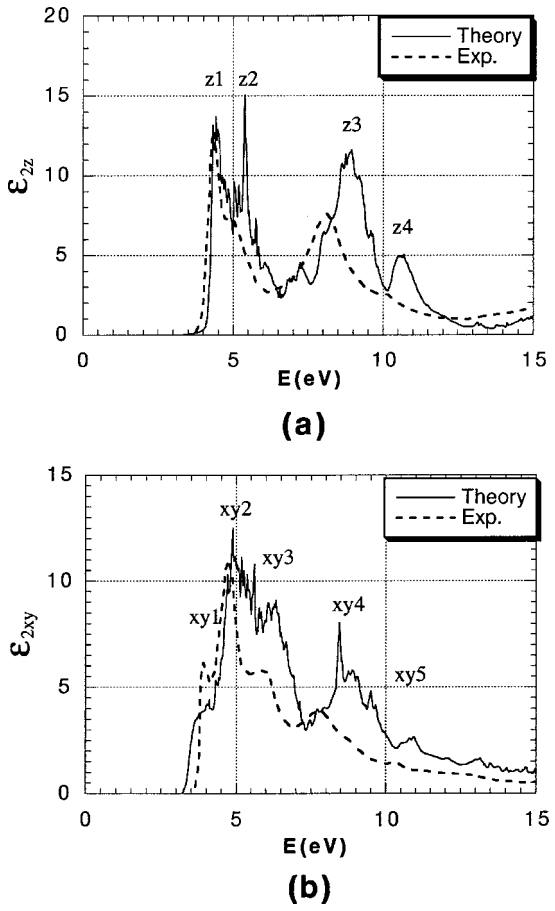

FIG. 8. Imaginary parts of the dielectric functions for polarization vectors (a) parallel and (b) perpendicular to the c axis. Solid lines and dashed lines are the present work and experiment (Ref. 11), respectively.

independent components, the z ($\mathbf{E}\|c$) component, ϵ_{2z} or ϵ_{1z}, and the xy ($\mathbf{E}\perp c$) component, ϵ_{2xy} or ϵ_{1xy}, which represents the average over the x and y components, using the k points only within the irreducible BZ. We treated the underestimated band gaps by using a scissors operator,[31] which displaces the empty and occupied bands relative to each other by a rigid shift of 1.14 eV, so that the minimum band gap becomes 3.14 eV in agreement with experiment. The experimental dielectric functions, measured for the single crystals of anatase using synchrotron orbital radiation,[11] are taken as comparison.

Very good agreement with experiment is obtained for the dielectric functions in both components. In particular, the positions and overall strengths of the peaks in the lower energy region reproduce experiment very well—which was not realized by the OLCAO results. The dielectric constants at $\omega\rightarrow 0$ are $\epsilon_{xy}(0)=5.97$ and $\epsilon_z(0)=5.57$, which show consistent agreement with an experimental value of 5.62,[32] suggesting that the choice of the scissors operator is reasonable.

In a higher energy region (>7 eV), however, the calculated peak positions are located at higher energies than experiment by 0.8–1.0 eV. Similar results were reported in calculations for the rutile structure, where good agreement with experiment was obtained in a higher (>6 eV) energy region *without* any correction to the LDA band gap, while the peak positions in the lower energy region were lower than experiment by about 1 eV.[4] This situation of the excitation energies in LDA is not usual for simple semiconductors such as Si, Ge, and GaAs, where LDA with the scissors operator works well to yield proper excitation energies in a wide energy range.[31] One reason to explain the problem in TiO_2 could be found in the unphysical self-interaction effect in LDA which is considered one of the origins of its band-gap underestimation.[33] The peaks in the lower and higher energy regions of ϵ_2 correspond to absorptive transitions from the valence bands to the t_{2g} and e_g orbitals in the conduction bands, respectively. The more localized the electron, the more the self interaction would be involved. Thus, the t_{2g} orbitals in the conduction bands, which are less hybridized with O and are relatively localized about Ti atoms, may be affected more by the larger self-interaction—and, hence, are lowered in energy relative to the e_g conduction bands.

A strong calculated optical anisotropy near the absorption edge has been observed as in Fig. 8. We have examined the major peaks near the absorption edge in Fig. 8 looking at the corresponding interband transitions as shown in Fig. 10. As seen in Sec. III A, the bottom of the conduction bands are dominantly the d_{xy} orbitals, to which transitions from the p_π states are dipole forbidden for the $\mathbf{E}\|c$ polarization but dipole allowed for the $\mathbf{E}\perp c$ polarization. The transitions of $z1$ and $z2$ are allowed since the final states in the conduction bands include d_{yz} or d_{zx} character, as seen in Fig. 4. By contrast, the experimental dielectric functions in Fig. 8 show a rather weak anisotropy at the absorption edge. It was suggested in Ref. 11 that the absorption edge was quite sensitive to the parameters employed for the K-K transformation to derive the experimental dielectric functions from the reflectivity measurements. Indeed, more direct measurements[16] of the optical absorption near the absorption edge for the single-

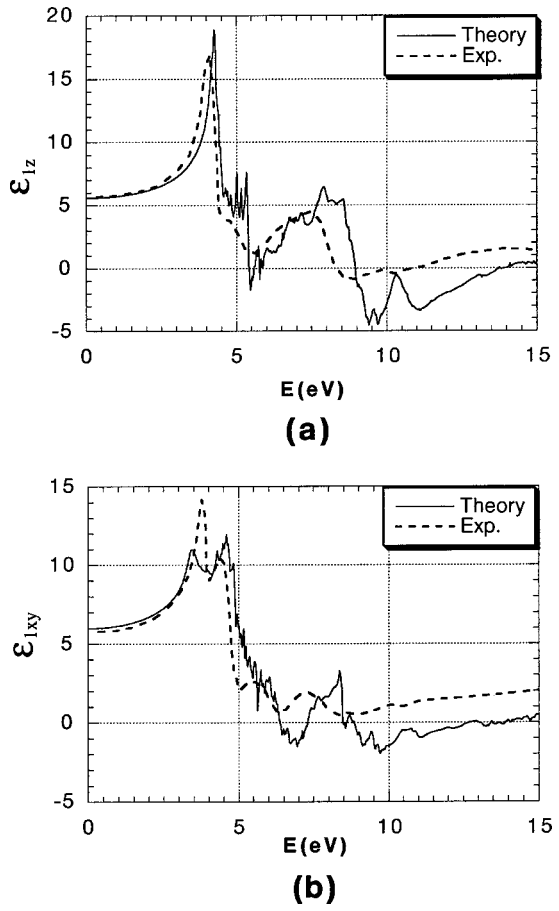

FIG. 9. The same quantities as in Fig. 8, but for the real parts.

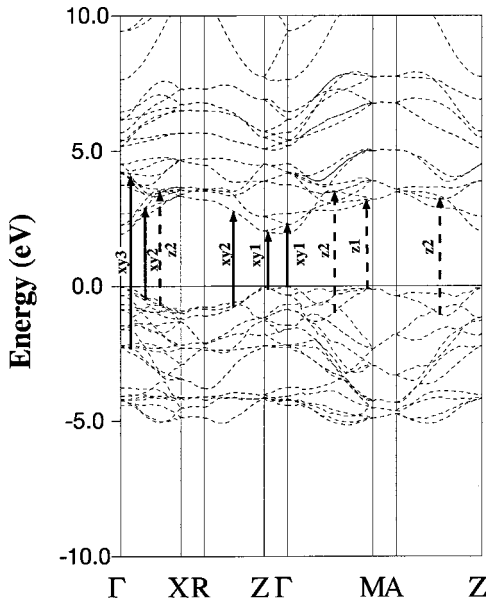

FIG. 10. Major optical transitions which contribute to the peak structures in the dielectric functions, ϵ_{xy} (bold solid lines) and ϵ_z (bold dashed lines). The corresponding peak structures are defined in Fig. 8.

crystal anatase TiO_2 showed that: (i) anatase has a larger dichroism than rutile; (ii) the oscillator strength of the transition near the absorption edge for $\mathbf{E}\perp c$ is about one order of magnitude larger than that for $\mathbf{E}\|c$; (iii) the $\mathbf{E}\perp c$ and $\mathbf{E}\|c$ absorption edges are assigned to be direct and indirect transitions, respectively; (iv) the excitons in anatase are concluded to be self trapped while those in rutile are free. All these results are consistent with the present calculations. In fact, the character of the bottom of the conduction bands, the isolated d_{xy} orbitals, confines the charge-transfer excitons at the lattice points. The coordination of the rutile structure, on the other hand, allows the excitons to be free since a nontrivial metal-metal interaction exists, as discussed in Sec. III A.

It should be noted that exciton effects often strongly modify the optical structures near the absorption edge within the one-electron theory used.[34–36] In elemental semiconductors like the group IV and III-V, by including the exciton effects, the first peak (interpreted as the $M1$-type van Hove singularity[37]) is enhanced and sharpened, while the second peak (the $M2$-type van Hove singularity) is weakened and smoothed out, demonstrating a significant improvement on the results obtained by the one-electron theory. By introducing the exciton effects in the present case, the relatively weak $xy1$ structure in Fig. 8, which is the direct transition and considered to be the $M1$-type van Hove singularity, may be enhanced, along with some reduction of the absorption in the region where the negative reduced mass of excitons is observed,[25] e.g., the $xy3$ structure. In the previous calculations for rutile TiO_2,[4] a disagreement of the first peak in ϵ_2 for $\mathbf{E}\|c$ with experiment was explained by possible exciton effects, though no additional evidence for this argument has been reported. In Elliott's theory,[38,25] the contribution to the imaginary part of the dielectric function due to exciton absorption at $\omega\sim\omega_g$ is proportional to μ^2/ϵ_0, where ω_g is the band gap and μ is the reduced mass of the exciton. Considering that the effective mass of anatase is smaller than that of rutile ($m_e^*\sim 1m_0$ for anatase[13] and $m_e^*\sim 8-20m_0$ for rutile[39,40]), and that their dielectric constants are comparable (5.62 for anatase and 6.33 for rutile[31]), we may expect the exciton effects of the continuum in anatase would be less significant than those in rutile.

IV. SUMMARY AND CONCLUSIONS

We have presented first-principles calculations of the electronic structure of anatase TiO_2 using the highly precise FLAPW method. The fully optimized structure was obtained by minimization of the total energy and atomic forces. The bond lengths obtained agree to within 2% of the experimental values; further improvement may be possible, e.g., by employing the GGA scheme. Very good agreement with experiment for the O-Ti-O angle, u, and c/a demonstrates the high accuracy of our approach. We investigated band structure, densities of states, and charge densities, and interpreted their features in terms of the bonding structure in the molecular orbital picture. Optical properties calculated within the dipole approximation showed that the dielectric functions agree with recent experiments on single crystals of anatase TiO_2. The disagreement of the peak positions of the dielectric functions in a higher energy region, however, suggests that a more sophisticated method going beyond the scissors operator to describe the quasiparticle spectrum of TiO_2 is required. A significant optical anisotropy in the components parallel and perpendicular to the c-axis near the absorption

edge was demonstrated. An inspection of interband transitions and character of the electronic structure showed that this large dichroism results from the existence of nonbonding d_{xy} states located at the bottom of the conduction bands and of non-bonding O p_π states located at the top of the conduction bands, which allows the direct dipole transitions to dominate for the $\mathbf{E} \perp c$ polarization.

ACKNOWLEDGMENTS

We thank J. Yu, T. Morikawa, and T. Ohwaki for helpful discussions. The calculations were performed at TOYOTA CRDL, Inc., on the NEC SX4 machine. The work of A. J. Freeman was supported by the DOE (Grant No. DF-FG02-88ER45372).

[1] A. Fujishima and K. Honda, Nature (London) **238**, 37 (1972).
[2] M. Grätzel, Comments Inorg. Chem. **12**, 93 (1991).
[3] K.I. Hadjiivanov and D.K. Klissurski, Chem. Soc. Rev. **25**, 61 (1996).
[4] K.M. Glassford and J.R. Chelikowsky, Phys. Rev. B **46**, 1284 (1992).
[5] P.I. Sorantin and K. Schwarz, Inorg. Chem. **31**, 567 (1992).
[6] M. Ramamoorthy, R.D. King-Smith, and D. Vanderbilt, Phys. Rev. B **49**, 7709 (1994).
[7] P.J.D. Lindan, N.M. Harrison, M.J. Gillan, and J.A. White, Phys. Rev. B **55**, 15 919 (1997).
[8] S.P. Bates, G. Kresse, and M.J. Gillan, Surf. Sci. **385**, 386 (1997).
[9] J. Goniakowski, J.M. Holender, L.N. Kantorovich, M.J. Gillan, and J.A. White, Phys. Rev. B **53**, 957 (1996).
[10] H. Berger, H. Tang, and F. Lévy, J. Cryst. Growth **130**, 108 (1993).
[11] N. Hosaka, T. Sekiya, C. Aatoko, and S. Kurita, J. Phys. Soc. Jpn. **66**, 877 (1997).
[12] R. Sanjinés, H. Tang, H. Berger, F. Gozzo, G. Margaritondo, and F. Lévy, J. Appl. Phys. **75**, 2945 (1994).
[13] H. Tang, K. Prasad, R. Sanjinés, P.E. Schmid, and F. Lévy, J. Appl. Phys. **75**, 2042 (1994).
[14] H. Tang, H. Berger, P.E. Schmid, F. Lévy, and G. Burri, Solid State Commun. **23**, 161 (1977).
[15] L. Forro, O. Chauvet, D. Emin, L. Zuppiroli, H. Berger, and F. Lévy, J. Appl. Phys. **75**, 633 (1994).
[16] H. Tang, F. Lévy, H. Berger, and P.E. Schmid, Phys. Rev. B **52**, 7771 (1995).
[17] A. Fahmi, C. Minot, B. Silvi, and M. Causá, Phys. Rev. B **51**, 13 023 (1995).
[18] J.K. Burdett, T. Hughbanks, G.J. Miller, J.W. Richardson, Jr., and J.V. Smith, J. Am. Chem. Soc. **109**, 3639 (1987).
[19] Shang-Di Mo and W.Y. Ching, Phys. Rev. B **51**, 13 023 (1995).
[20] E. Wimmer, H. Krakauer, M. Weinert, and A.J. Freeman, Phys. Rev. B **24**, 864 (1981), and references therein; M. Weinert, E. Wimmer, and A.J. Freeman, *ibid.* **26**, 4571 (1982); H.J.F. Jansen and A.J. Freeman, *ibid.* **30**, 561 (1984).
[21] L. Hedin and B.I. Lundqvist, J. Phys. C **4**, 2064 (1971).
[22] R. Yu, D. Singh, and H. Krakauer, Phys. Rev. B **45**, 8671 (1991).
[23] W. Mannstadt and A.J. Freeman, Phys. Rev. B **55**, 13 298 (1997).
[24] H.J. Monkhorst and J.D. Pack, Phys. Rev. B **13**, 5188 (1976).
[25] P.Y. Yu and M. Cardona, *Fundamentals of Semiconductors* (Springer, Berlin, 1996).
[26] D. Jepsen and O.K. Anderson, Solid State Commun. **9**, 1763 (1971); G. Lehmann and M. Taut, Phys. Status Solidi **54**, 469 (1972).
[27] Y. Petroff, M. Balkanski, J.P. Walter, and M.L. Cohen, Solid State Commun. **7**, 459 (1969).
[28] J.K. Burdett, T. Hughbanks, G.J. Miller, J.W. Richardson, Jr., and J.V. Smith, J. Am. Chem. Soc. **109**, 3639 (1987).
[29] J.P. Perdew and Y. Wang, Phys. Rev. B **45**, 13 244 (1992).
[30] R.M. Dreizler and E.K.U. Gross, *Density Functional Theory, An Approach to the Quantum Many-Body Problem* (Springer-Verlag, Berlin, 1990).
[31] G.A. Baraff and M. Schlüter, Phys. Rev. B **30**, 3460 (1984); R. Del Sole and R. Girlanda, *ibid.* **48**, 11 789 (1993).
[32] S.H. Wemple, J. Chem. Phys. **67**, 2151 (1977).
[33] J.P. Perdew and A. Zunger, Phys. Rev. B **23**, 5048 (1981).
[34] M. Rohlfing and S.G. Louie, Phys. Rev. Lett. **81**, 2312 (1998).
[35] S. Albrecht, L. Reining, R. Del Sole, and G. Onida, Phys. Rev. Lett. **80**, 5048 (1998).
[36] L.X. Benedict and E.L. Shirley, Phys. Rev. B **59**, 5441 (1999).
[37] C.S. Wang and B.M. Klein, Phys. Rev. B **24**, 3417 (1981).
[38] R.J. Elliott, Phys. Rev. **108**, 1384 (1957).
[39] J. Pascual, J. Camassel, and H. Mathieu, Phys. Rev. Lett. **39**, 1490 (1977).
[40] H.P.R. Frederikse, J. Appl. Phys. **32**, 2211 (1961).